Abdominal Imaging

Published online: 19 February 2014

Abdom Imaging (2014) 39:744–752
DOI: 10.1007/s00261-014-0107-z

Pancreatic adenocarcinoma: a pilot study of quantitative perfusion and diffusion-weighted breath-hold magnetic resonance imaging

Hyunki Kim,[1,2,6,9] Pablo J. Arnoletti,[7] John Christein,[3] Martin J. Heslin,[3] James A. Posey III,[4] Amol Pednekar,[8] T. Mark Beasley,[5] Desiree E. Morgan[1,6]

[1]Departments of Radiology, University of Alabama at Birmingham, Birmingham, AL 35294-0019, USA
[2]Biomedical Engineering, University of Alabama at Birmingham, Birmingham, AL 35294-0019, USA
[3]Department of Surgery, University of Alabama at Birmingham, Birmingham, AL 35294-0019, USA
[4]Department of Medicine, University of Alabama at Birmingham, Birmingham, AL 35294-0019, USA
[5]Department of Biostatistics, University of Alabama at Birmingham, Birmingham, AL 35294-0019, USA
[6]Comprehensive Cancer Center, University of Alabama at Birmingham, Birmingham, AL 35294-0019, USA
[7]The Center for Specialized Surgery, Orlando, FL 32804, Philips
[8]Medical Systems, Bothell, WA 98021, USA
[9]G082 Volker Hall 1720 2nd Avenue South, Birmingham, AL 35294-0019, USA

Abstract

Purpose: To confirm the feasibility of breath-hold DCE-MRI and DWI at 3T to obtain the intra-abdominal quantitative physiologic parameters, K^{trans}, k_{ep}, and ADC, in patients with untreated pancreatic ductal adenocarcinomas.
Methods: Diffusion-weighted single-shot echo-planar imaging (DW-SS-EPI) and dynamic contrast-enhanced (DCE) MRI were used for 16 patients with newly diagnosed biopsy-proven pancreatic ductal adenocarcinomas. K^{trans}, k_{ep}, and apparent diffusion coefficient (ADC) values of pancreatic tumors, non-tumor adjacent pancreatic parenchyma (NAP), liver metastases, and normal liver tissues were quantitated and statistically compared.
Results: Fourteen patients were able to adequately hold their breath for DCE-MRI, and 15 patients for DW-SS-EPI. Four patients had liver metastases within the 6 cm of Z axis coverage centered on the pancreatic primary tumors. K^{trans} values (10^{-3} min^{-1}) of primary pancreatic tumors, NAP, liver metastases, and normal liver tissues were 7.3 ± 4.2 (mean ± SD), 25.8 ± 14.9, 8.1 ± 5.9, and 45.1 ± 15.6, respectively, k_{ep} values (10^{-2} min^{-1}) were 3.0 ± 0.9, 7.4 ± 3.1, 5.2 ± 2.0, and 12.1 ± 2.8, respectively, and ADC values (10^{-3} mm^2/s) were 1.3 ± 0.2, 1.6 ± 0.3, 1.1 ± 0.1, and 1.3 ± 0.1, respectively. K^{trans}, $k_{ep,}$ and ADC values of primary pancreatic tumors were significantly lower than those of NAP ($p < 0.05$), while K^{trans} and k_{ep} values of liver metastases were significantly lower than those of normal liver tissues ($p < 0.05$).
Conclusions: 3T breath-hold quantitative physiologic MRI is a feasible technique that can be applied to a majority of patients with pancreatic adenocarcinomas.

Key words: DCE-MRI—DWI—Pancreatic adenocarcinoma

Correspondence to: Hyunki Kim; *email:* Hyunki@uab.edu

There is much interest in the use of quantitative imaging as a surrogate biomarker in oncologic applications [1–3], both as a measure of pharmacodynamic tumor response and also as a prognosticator of clinical outcome (both tumor response and patient survival). Two physiologic magnetic resonance imaging (MRI) techniques, dynamic contrast-enhanced MRI (DCE-MRI) and diffusion-weighted imaging (DWI) have been actively utilized as imaging biomarkers for many extra-abdominal cancers in human subjects, but there has been limited application for intra-abdominal diseases mainly due to motion. More recently, high-field-strength MR scanners have allowed performing these types of sequences with improved temporal resolution, lowering the incidence of motion artifacts [4], although increased susceptibility

artifacts and the limitation of maximum specific absorption rate (SAR) are still concerns [5].

DCE-MRI represents a non-invasive measure of tumor microvasculature and encompasses a pharmacokinetic model using signal intensity changes over time following MR contrast injection. To accurately calculate the concentration of MR contrast in vivo, pre-contrast T1 maps must be obtained. However, since T1 maps and DCE-MR images are acquired at different time points, while internal organs move in coordination with breathing, accurate image co-registration is essential. Also, the dynamic change of the contrast concentration in an aortic region (i.e., arterial input function (AIF)) must be determined to quantitate pharmacokinetic parameters such as K^{trans} and k_{ep} values. Ideally, the AIF is measured with a 1–2 s sampling rate [6]. K^{trans} represents the transfer rate of an MR contrast from blood plasma to the extravascular extracellular space (EES) per unit volume of tissue, while k_{ep} represents the reverse transfer rate of the MR contrast from the EES to blood plasma.

One of the important issues with respect to abdominal DCE-MRI is the tradeoff between breath-hold and free-breathing techniques. The motion of abdominal organs can be minimized by suspending respiration, but pancreatic cancer patients cannot typically perform breath-holds longer than 30 s. Thus, breath holding after inhalation must be repeated at intervals during the entire length of the DCE-MR image acquisition, and severe motion artifact is often observed when patients exhale. However, the wash-in of a gadolinium-based MR contrast agent within abdominal organs usually occurs approximately 20 s after the initiation of IV contrast administration [7, 8]; therefore, the wash-in rate may be monitored with high accuracy without the need for image co-registration if a breath-hold technique is employed. During free breathing, abdominal organs move continuously but slowly and regularly. The displacement of target regions in free-breathing DCE-MR images can be compensated using an automated image co-registration technique, if temporal resolution is sufficiently high [9]. Quantitative DCE-MRI has been recently evaluated for patients with pancreatic adenocarcinomas in both breath-hold [10] and free-breathing modes [8]; significantly lower K^{trans} and k_{ep} values of pancreatic tumors were observed when compared with those of non-tumor adjacent pancreatic parenchyma (NAP) regardless of breathing mode, although the absolute values of the perfusion parameters were largely different between the two studies.

DWI is a method that measures hindered water diffusion in tissues, affected by cellular micro-viscosity, organelle, membrane, and molecular interaction. The magnitude of water diffusion is quantitatively represented with the apparent diffusion coefficient (ADC). In general, neoplastic tissues have impaired water diffusion, which is reflected by lower ADC values [11]. In the abdomen, ADC values have been used to differentiate benign from malignant lesions in the liver [12, 13] as well as to differentiate intra-pancreatic accessory spleens (IPAS) from pancreatic adenocarcinomas [14]. ADC values of pancreatic tumors are significantly lower than those of benign pancreatic tissues [15].

The purpose of this study was to confirm the feasibility of breath-hold DCE-MRI and DWI at 3T to obtain the intra-abdominal quantitative physiologic parameters, K^{trans}, k_{ep}, and ADC, in patients with untreated pancreatic ductal adenocarcinomas. Also, the relative values of the lesions (pancreatic tumors or liver metastases) to reference tissues (NAP or normal liver tissue) were further investigated as more reliable measures.

Materials and methods

This prospective pilot study received approval from the full-convened institutional review board of our institution. All subjects signed informed consent, and the health insurance portability and accountability act was strictly observed.

Subjects

Sixteen subjects (14 white, 2 African American), ten men and six women with a mean age of 64 years, were accrued. All subjects had newly diagnosed, biopsy-proven pancreatic adenocarcinomas, and agreed to undergo pre-treatment MRI. Collected clinical data included tumor stage, grade, primary tumor location, single longest axis size measurement, and the presence of pancreatitis (as determined by histology in the surgically resected specimens).

MRI

All subjects were examined on a single 3T clinical MR system (Philips Achieva, Philips Medical Systems, Best, the Netherlands). Routine anatomic pancreatic MRI included localizers, respiratory-triggered turbo spin echo (TSE) fat-suppressed images through the upper abdomen, T1-weighted 3-dimensional (3D)-spoiled gradient echo (GRE) fat-suppressed breath-hold images at end inspiration, and MR cholangiopancreatography using high resolution 3D respiratory triggered TSE. Breath-hold DW single-shot echo-planar imaging (DW-SS-EPI) was performed with two b values of 0 and 700 s/mm^2 with following parameters: repetition time/echo time (TR/TE) = 3666/65 ms, field of view (FOV) = 38 × 26 cm, number of excitation (NEX) = 1, thickness/gap = 4/1 mm, and matrix = 128/102 (interpolated to 256 × 256). DW images with the higher b value were acquired in three orthogonal directions. A total of 24

slices (4 images per slice) were obtained during 20 s of breath-hold. T1 maps were created by performing three separate breath-hold 3D-spoiled gradient echo T1-weighted axial sequences with flip angles of 5, 10, and 15°, respectively, with following parameters: TR/TE = 5/2.3 ms, FOV = 40 × 40 cm, NEX = 1, thickness/gap = 6/0 mm, matrix = 192/154 (interpolated to 256 × 256), and SENSE factor = 2. A total of 10 slices were obtained during 20 s of breath hold for imaging with each flip angle. DCE-MRI employed 3D fast field echo sequence; the same acquisition parameters as those for creating T1 maps were used, but with a fixed flip angle of 15°. A total of 92–96 images were continuously acquired with temporal resolution of 2.1 s after intravenous injection of 0.1 mmol/kg of gadoteridol (Bracco Diagnostics Inc., Princeton, NJ) with 20-ml saline flush at the rate of 2 mL/s. During DCE-MRI, patients were instructed to perform breath-hold in maximal end inspiration for as long as possible, and then repeat similar breath-holds as feasible.

Image analysis

For correcting motion in DCE-MR images, three image-processing techniques were employed: unwarping, median filtering, and curve fitting [16]. For unwarping, the boundary of a patient's body above the paravertebral muscle and abdominal aorta was determined in each DCE-MR image. Then, the boundary in each DCE-MR image was unwarped to match with the boundary in the baseline image (acquired prior to gadoteridol injection), and all pixels within the boundary were relocated accordingly. Thereafter, median filtering and curve fitting were applied to the entire body region including the paravertebral muscle and abdominal aorta. Assuming patients were able to do breath-hold for at least 20 s, median filtering and curve fitting were applied for the signal curve of each pixel from 20 s after obtaining the baseline image; one-dimensional median filtering (window: 5) was applied first, and then the best-fit 5th-order polynomial curve was determined. T1 maps were also unwarped as described above and co-registered with DCE-MR images.

Tofts' two-compartment pharmacokinetic model was employed to calculate volume transfer constant (K^{trans}) and reverse efflux rate constant (k_{ep}) [17]. The modified general rate equation in a two-compartment model is

$$C_t(t) = v_p c_p(t) + \left(K^{trans} + v_p k_{ep}\right) \int_0^t C_p(t')\mathrm{d}t' - k_{ep} \int_0^t C_t(t')\mathrm{d}t',$$

where $C_t(t)$, $C_p(t)$, and v_p represent contrast concentration in tissue at t time, contrast concentration in blood plasma at t time, and fraction occupied by blood plasma, respectively. $C_p(t)$, also known as arterial input function (AIF), was obtained by measuring the change of gadoteridol concentration within the abdominal aortic region. Relaxivity of gadoteridol at 3T was estimated to 3.09 s^{-1} mM^{-1}, as previously reported [18]. Two-dimensional median filtering (window: 3 × 3) was applied for K^{trans} and k_{ep} maps to further reduce noise.

In DW image analysis, ADC values were calculated by ADC = $\ln(I_1/I_2)/(b_2 - b_1)$, where I_1 was the intensity of each pixel in DW images obtained with the lower b value (b_1), and I_2 was that with the higher b value (b_2); the DW images with the higher b value in three orthogonal directions were averaged prior to calculating ADC values. Two-dimensional median filtering (window: 3 × 3) was also applied for ADC maps to suppress noise.

The regions of interest (ROIs) such as pancreatic tumors, non-tumor adjacent pancreatic parenchyma (NAP), liver metastases, and normal liver tissues were determined based on the signal-intensity difference between the ROIs and background in diffusion-weighted and contrast-enhanced MR images to retrieve diffusion and perfusion parameters, respectively, by a board-certified radiologist specializing in abdominal imaging for 18 years. The boundary of each ROI was manually drawn and segmented using ImageJ (version 1.47n; National Institutes of Health, Bethesda, MD), and the physiological parameters (K^{trans}, k_{ep}, ADC) within each ROI were averaged. The motion correction in DCE-MR images and the quantification of physiological parameters were implemented using computer software developed with Labview, version 2010 (National Instruments Co., Austin, TX).

Statistical analysis

One-way ANOVA (analysis of variance) was performed to compare the physiological parameters in four different regions including pancreatic tumors, NAP, liver metastases, and normal liver tissues, while Bonferroni correction was applied for multiple comparisons [19]. The relative values of the lesions (pancreatic tumors or liver metastases) to reference tissues (NAP or normal liver tissues) were also compared using one-way ANOVA. p values less than 0.05 were considered significant, and data were presented as mean ± standard deviation. All analyses were performed using SAS, version 9.2 (SAS Institute Inc., Cary, NC).

Results

Table 1 shows the characteristics of primary pancreatic tumors according to disease stage at diagnosis. Six subjects presented with synchronous liver metastases, three had locally advanced tumors, and seven presented with resectable disease. Nine subjects had pancreatic tumors

in the head of the pancreas, two in the neck, two in the body, and three in the tail. The range of single longest axis tumor measurement was 1.4–4.8 cm, without statistical difference among disease stages. One of the subjects with locally advanced pancreatic cancer was successfully down staged by neoadjuvant chemoradiation therapy and underwent surgical resection. Seven among eight surgical specimens demonstrated tumor-associated chronic pancreatic inflammation. The presence or degree of pancreatic inflammation in the unresected subjects could not be determined histologically, as biopsy was directed toward the tumor. Fifteen subjects held their breath successfully during DWI (94%), and fourteen subjects coordinated repeated breath holding successfully during DCE-MRI (88%). Two subjects had liver metastases out of the Z axis longitudinal field of view (limited to 6 cm) of the DCE-MR images. Two liver metastases of each subject with DCE-MRI evaluable metastatic pancreatic cancer were randomly selected and analyzed (i.e., a total of eight liver metastases were analyzed).

Table 1. Characteristics of primary pancreatic tumor according to disease stage at diagnosis

Diagnosis	Location of P tumor				Size (cm)	Pancreatitis		
	Head	Neck	Body	Tail		Yes	No	Unknown
Resectable PC	6	1	0	0	2.9±1.1	6	1	0
LA PC	1	0	1	1	3.7±1.0	1	0	2
MET PC	2	1	1	2	3.6±1.0	0	0	6

P tumor primary pancreatic tumor, *PC* pancreatic cancer, *LA* locally advanced, *MET* metastatic

Figures 1 and 2 shows representative motion-corrected DCE-MR images and parametric maps of a 59-year-old man with a resectable pancreatic adenocarcinoma and a 64-year-old man with multiple liver metastases, respectively. Figure 1A, B (or Fig. 2A, B) shows DCE-MR images (a) before (baseline image) and (b) at 30 s after gadoteridol injection, when a constant gray scale was applied. Figure 1C–E (Fig. 2C–E) presents the contrast concentration map at 30 s after gadoteridol injection, K^{trans} map, and k_{ep} map, respectively. Figure 1F (or Fig. 2F) shows contrast-enhancement curves averaged in the abdominal aorta (i.e., AIF), NAP, and pancreatic tumor (or normal liver tissue and metastasis) indicated in each subfigure. The mean initial peak of AIF in all 14 patients was 0.99 ± 0.18 mM, while the dip after the initial peak was 0.69 ± 0.14 mM.

Figure 3A, B presents box plots of the K^{trans} and k_{ep} values of primary pancreatic tumors, NAP, liver

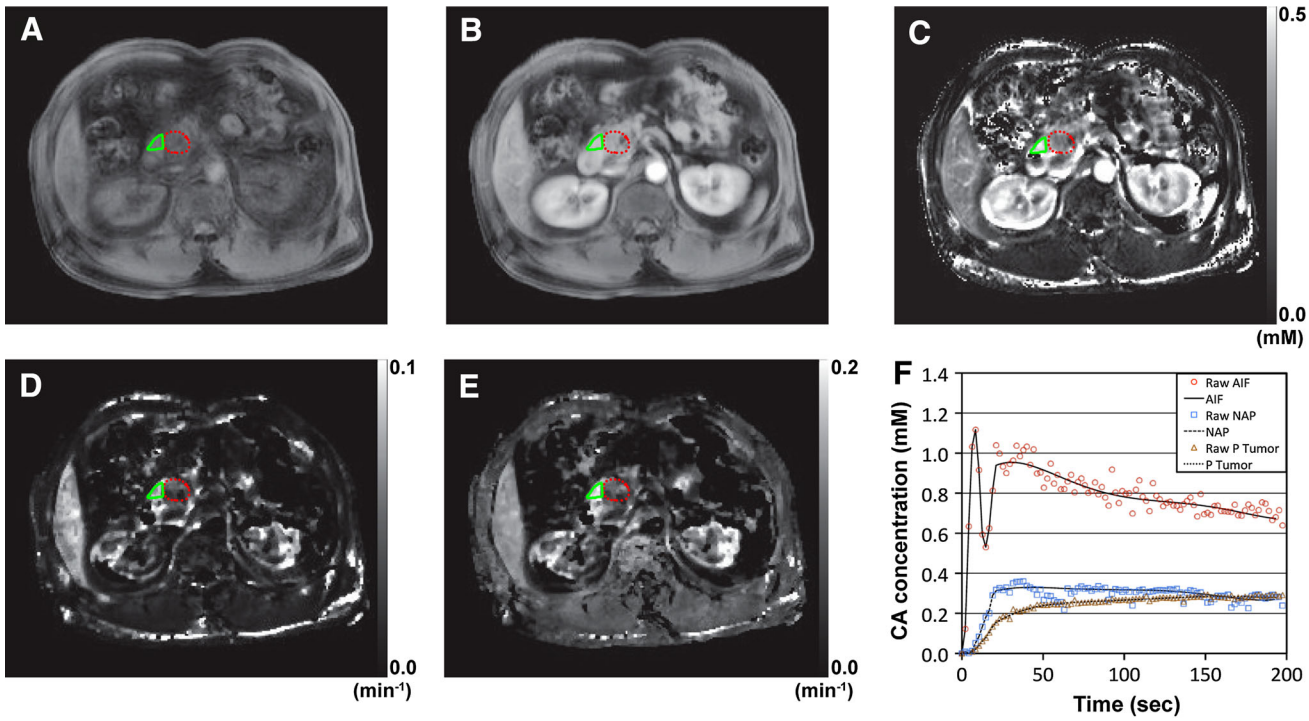

Fig. 1. Representative DCE-MR images, contrast concentration map, and parametric maps of a 59-year-old man with pancreatic adenocarcinoma. (**A**, **B**) DCE-MR images: **A** before and **B** at 30 s after contrast injection with constant *gray scale*. The regions of tumor and non-tumorous adjacent parenchyma are indicated with *red dotted* and *green solid lines*, respectively. **C** Contrast-agent concentration map at 30 s after contrast injection. **D** K^{trans} map. **E** k_{ep} map. **F** Contrast-agent (CA) enhancement curves averaged in aorta (i.e., arterial input function (AIF)), non-tumor adjacent parenchyma (NAP), and pancreatic tumor (P Tumor) before and after motion correction.

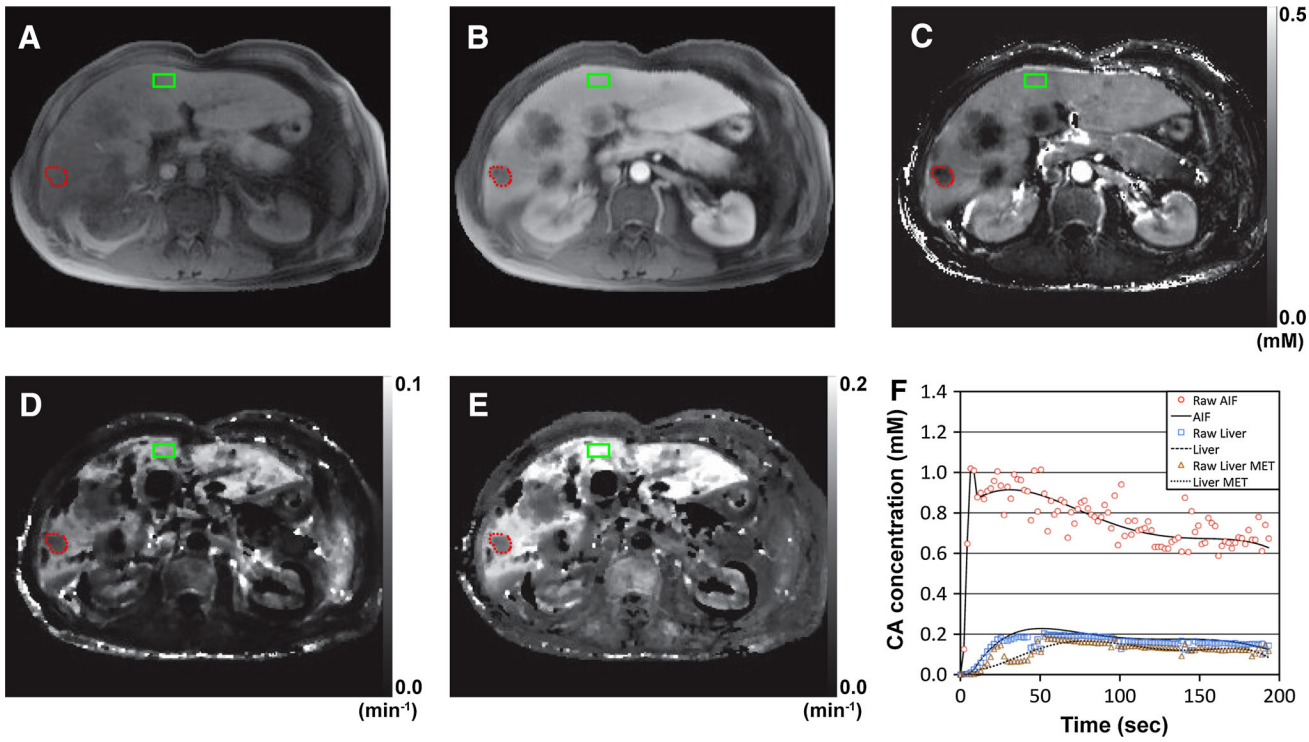

Fig. 2. Representative DCE-MR images, contrast concentration map, and parametric maps of a 64-year-old man with multiple liver metastases arising from pancreatic adenocarcinoma. (**A**, **B**) DCE-MR images: **A** before and **B** at 30 s after contrast injection with constant *gray scale*. The liver metastasis and normal liver tissue are indicated with *red dotted* and *green solid lines*, respectively. **C** Contrast-agent concentration map at 30 s after contrast injection. **D** K^{trans} map. **E** k_{ep} map. **F** Contrast-agent (CA) enhancement curves averaged in aorta (i.e., arterial input function (AIF)), normal liver tissues (liver), and liver metastases (liver MET) before and after motion correction.

metastases, and normal liver tissues, respectively. Each box represents the interquartile range, and the horizontal line within the box represents the median value. The whiskers attached on each box show the entire range of all values. Both the K^{trans} and k_{ep} values of primary pancreatic tumors and liver metastases were significantly lower than those of NAP or normal liver tissues ($p < 0.05$), but the K^{trans} and k_{ep} values of primary pancreatic tumors were not statistically different from those of liver metastases ($p > 0.05$). Figure 3C, D presents the K^{trans} and k_{ep} values of pancreatic tumors (or liver metastases) relative to those of NAP or normal liver tissues; the relative K^{trans} and k_{ep} values of primary pancreatic tumors were significantly lower when normal liver tissues were used as reference ($p < 0.05$).

Figure 4 shows representative DW images with b values of 700 and 0 s/mm^2 using a constant gray scale, in addition to ADC maps of two different patients: a 50-year-old man with a resectable pancreatic adenocarcinoma and a 70-year-old man with multiple liver metastases. Figure 5A demonstrates box plots of the ADC values of primary pancreatic tumors, NAP, liver metastases, and normal liver tissues. The ADC values of pancreatic tumors were significantly lower than those of NAP ($p = 0.0022$), but not different from those of normal liver tissues and liver metastases ($p > 0.05$). Figure 5B presents the ADC values of pancreatic tumors (or liver metastases) relative to those of NAP or normal liver tissues; no statistical significance was found among groups.

Table 2 summarizes the mean values of the physiologic parameters (K^{trans}, k_{ep}, and ADC) of pancreatic tumors, NAP, liver metastases, and normal liver tissues. Of interest, the coefficient of variance (CV) in k_{ep} values of the four tissues was 33.2%, which was lower than that in K^{trans} value (55.7%). Table 3 summarizes the mean values of the physiologic parameters of pancreatic tumors (or liver metastases) relative to those of NAP or normal liver tissues.

Discussion

The K^{trans} and k_{ep} values of primary pancreatic tumors were significantly lower than those of NAP, which was consistent with recently reported results [8, 10]. However, the mean values showed large difference among studies. Table 4 presents the comparison of three independently performed DCE-MRI studies. All three studies employed Tofts' two-compartment pharmacokinetic model to retrieve the perfusion parameters, but the mean

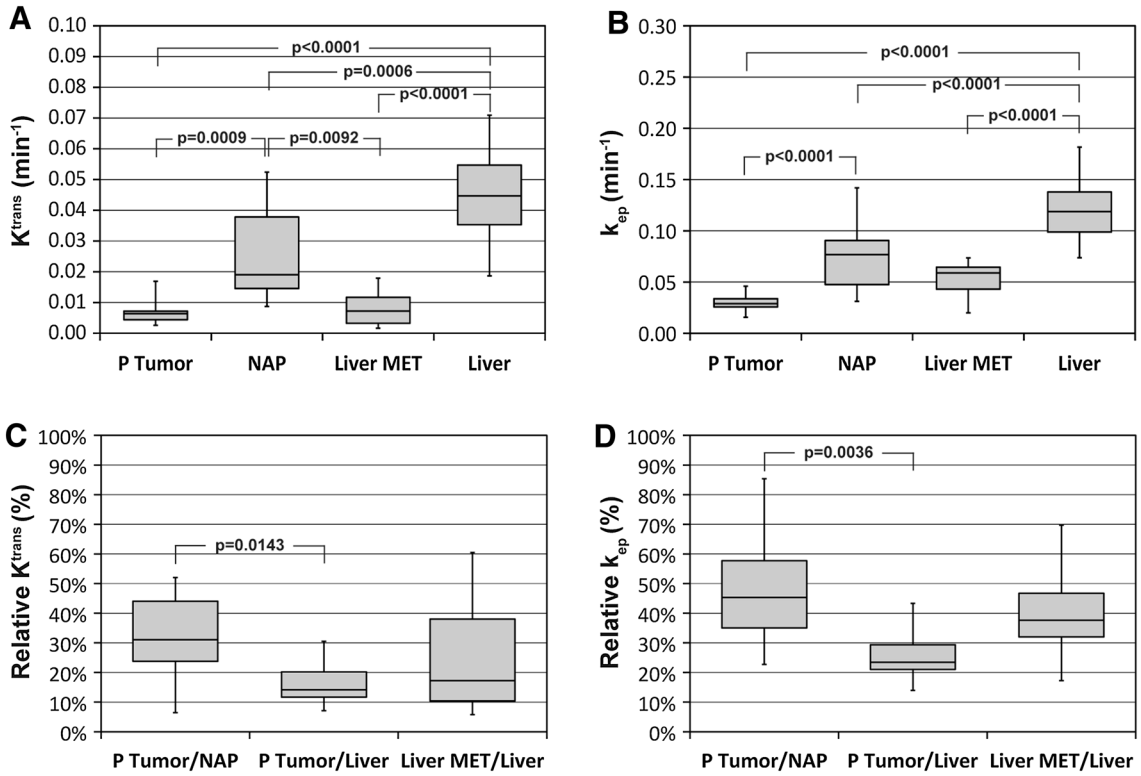

Fig. 3. *Box plots* showing perfusion parameters. **A** K^{trans} and **B** k_{ep} values of pancreatic tumors (P tumor), non-tumorous adjacent parenchyma (NAP), liver metastases (liver MET), and normal liver tissues (liver). **C** K^{trans} and **D** k_{ep} values of pancreatic tumors (or liver metastases) relative to those of non-tumorous adjacent parenchyma (NAP) and/or normal liver tissues (liver). Each *box* represents the interquartile range, the *horizontal line* within the box represents the median value, and the *whiskers* show the range of all values. *p* values were inserted when statistical significance was found between two groups.

K^{trans} value of pancreatic tumors in the current study was about sixfold smaller than that reported by Kim et al. [8] and about 240 fold smaller than that reported by Yao et al. [10]. The absolute values of the perfusion parameters may vary according to imaging parameters, contrast agents, and quantification methods [20], and that may explain the difference. In fact, it has been reported that commercially available perfusion analyzers yield different values with the same dynamic images [21, 22]. Furthermore, the physiochemical properties of a contrast agent affect the perfusion parameters as well. Gadoteridol (Prohance) has low viscosity (1.3 cP) relative to the other gadolinium-based MR contrast agents [23]; thus, it can be more easily mixed with blood before reaching the abdominal area, which may explain the lower initial peak of AIF (about 1 mM in average) than that of gadopentetate dimeglumine (Magnevist) (about 6 mM in average) [6]. Therefore, it seems pertinent to standardize DCE-MRI protocols to improve the reproducibility of the quantitated values. Alternatively, relative values may be utilized to assess tissue vasculature more reliably. We described the relative K^{trans} and k_{ep} values of the lesions compared with reference tissues such as NAP or normal liver tissues. The relative K^{trans} value of pancreatic tumor to NAP in this study (32%) was comparable with those of the two previous studies (14 and 44%). However, since NAP can have inflammation, fibrosis, and acinar cell loss [24], unaffected normal liver tissue may serve as a more reliable reference.

The ADC values of primary pancreatic tumors in this study ($1.3 \pm 0.2 \times 10^{-3}$ mm^2/s) were comparable with the values reported by Matsuki et al. [25], $1.4 \pm 0.2 \times 10^{-3}$ mm^2/s in eight patients with resectable pancreatic adenocarcinomas. Also, the ADC values of NAP in our population ($1.6 \pm 0.3 \times 10^{-3}$ mm^2/s) were similar to those ($1.5 \pm 0.1 \times 10^{-3}$ mm^2/s) reported in 14 patients with pancreatic exocrine dysfunction by Balci et al. [26]. In the current study, the mean ADC value of liver metastases was $1.1 \pm 0.1 \times 10^{-3}$ mm^2/s, which was about 17% lower than that of normal liver tissues ($1.3 \pm 0.1 \times 10^{-3}$ mm^2/s), but no statistical significance was found ($p = 0.1078$). Bruegel et al. [27] also reported similar results; the mean ADC value of liver metastases was $1.2 \pm 0.3 \times 10^{-3}$ mm^2/s, and that of normal liver tissues was $1.2 \pm 0.2 \times 10^{-3}$ mm^2/s, although the primary sites of the metastases comprises various abdominal organs including the pancreas. However, all the studies were performed on 1.5 T units. At the higher

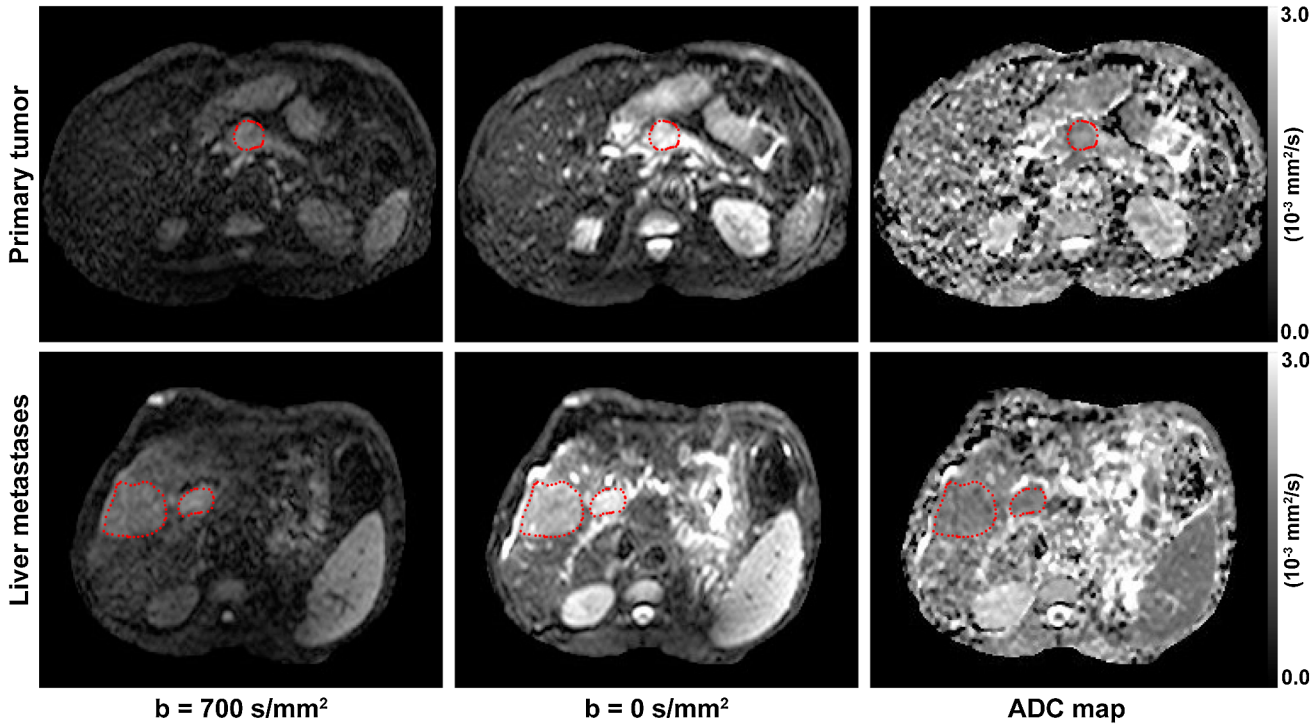

Fig. 4. Representative diffusion-weighted images of a 50-year-old man with pancreatic adenocarcinoma and a 70-year-old man with multiple liver metastases arising from pancreatic adenocarcinoma at two *b* values of 700 and 0 s/mm^2 with constant *gray scale*, and ADC maps. The tumor regions are indicated with *red dotted lines*.

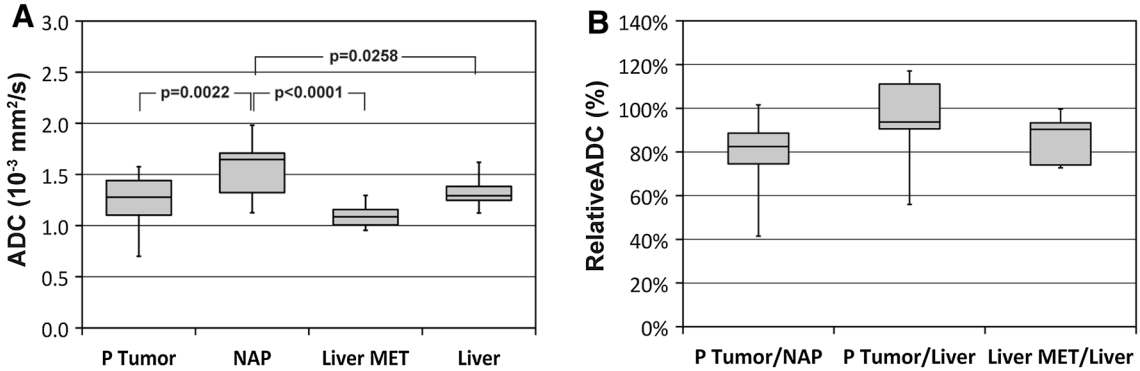

Fig. 5. *Box plots* showing apparent diffusion coefficient (ADC) values. **A** ADC values of pancreatic tumors (P Tumor), non-tumorous adjacent parenchyma (NAP), and liver metastases (liver MET), and normal liver tissues (liver). **B** ADC values of pancreatic tumors (or liver metastases) relative to those of non-tumorous adjacent parenchyma and/or normal liver tissues. Each *box* represents the interquartile range, the *horizontal line* within the box represents the median value, and the *whiskers* show the range of all values. *p* values were inserted when statistical significance was found between two groups.

Table 2. Physiological parameters of primary pancreatic tumors (P tumor), non-tumorous adjacent parenchyma (NAP), liver metastases (liver MET), and normal liver tissues (liver)

P tumor	NAP	Liver MET	Liver
K^{trans} (10^{-3} min^{-1})	7.3±4.2	8.1±5.9	45.1±15.6
k_{ep} (10^{-2} min^{-1})	3.0±0.9	5.2±2.0	12.1±2.8
ADC (10^{-3} mm^2/s	1.3±0.2	1.1±0.1	1.3±0.1

Table 3. Physiological parameters of primary pancreatic tumors (P tumor) or liver metastases (liver MET) relative to those of non-tumorous adjacent parenchyma (NAP) and/or normal liver tissues (liver)

P tumor/NAP	P tumor/Liver	Liver MET/liver
Relative K^{trans} (%)	32±14%	26±21%
Relative k_{ep} (%)	45±17%	41±18%
Relative ADC (%)	81±14%	86±11%

Table 4. Major differences among recently published two studies by Kim et al. [8] and Yao et al. [10] and our current study are presented with the K^{trans} and k_{ep} values (mean ± SD) of primary pancreatic cancer (PC) or non-tumor adjacent pancreatic parenchyma (NAP)

Study	Patient number	Scanner	Quantification software	Contrast agent	Pulse sequence	Breathing mode	PC K^{trans} (min^{-1})	PC k_{ep} (min^{-1})	NAP K^{trans} (min^{-1})	NAP k_{ep} (min^{-1})
Kim et al. [8]	24	3T TIM Trio (Siemens)	Tissue 4D	Magnevist	3D radial VIBE	Free breathing	0.042 ± 0.023	0.761 ± 0.529	0.293 ± 0.234	4.269 ± 3.425
Yao et al.[10]	40	3T Signa HDx (GE)	CINE tool	Magnevist	3D Lava	Breath-hold	1.663 ± 0.25	2.526 ± 1.55	3.769 ± 1.67	5.636 ± 1.64
Current study	14	3T Achieva (Philips)	Lab-made	Prohance	3D FFE	Breath-hold	0.007 ± 0.004	0.030 ± 0.009	0.026 ± 0.015	0.074 ± 0.031

field strength, susceptibility artifacts and geometrical distortions may be more problematic especially in DW-SS-EPI. We found a 14.4% coefficient of variance in ADC values, which is fairly comparable with what Braithwaite et al. [28] reported at 3T (14.7%). Malyarenko et al. reported that the reproducibility of ADC measurement at the magnetic isocenter of clinical MR scanners (1.5 T or 3 T) was within 3%. However, microperfusion in a tissue can affect ADC values when low *b* values (less than 300 s/mm^2) are used [29]; thus, higher *b* values (more than 2 *b* values ideally) will be necessary to improve the reproducibility of ADC measurement.

The importance of quantitative DWI and DCE-MRI may lie in the early detection of response to therapy that may enable precision medicine. These quantitative physiologic measures have been utilized to detect early tumor responses following chemo- and/or radiation therapy for patients with various cancers [30–35], and this may allow clinicians to tailor therapeutic strategies for the individual patient. Also, the baseline values of these physiologic parameters could be used to optimize therapeutic strategy; for example, anti-angiogenic drugs may be preferred in patients with well-perfused tumors and anti-stromal drugs in patients with hypo-perfused tumors.

In conclusion, 3 T breath-hold quantitative physiologic MRI is a feasible technique that could be applied to a majority of patients with pancreatic adenocarcinomas. We encountered limitations of patient incapability with required breath holding in two patients, and the small *Z* axis coverage is limiting with regard to full coverage of the liver for metastasis evaluation. The standardization of imaging protocols incorporating DCE-MRI is a necessary step to improve the reproducibility of quantitative measures for evaluation of therapeutic response. The relative physiologic parameters proposed in this study need further validation in patients receiving chemotherapeutic treatment.

Grant support Research Initiative Pilot Award from the Department of Radiology at UAB and NIH grant 2P30CA013148.

References

1. Evelhoch J, Garwood M, Vigneron D, et al. (2005) Expanding the use of magnetic resonance in the assessment of tumor response to therapy: workshop report. Cancer Res 65(16):7041–7044. doi:10.1158/0008-5472.CAN-05-0674
2. Hoffman JM, Gambhir SS (2007) Molecular imaging: the vision and opportunity for radiology in the future. Radiology 244(1):39–47. doi:10.1148/radiol.2441060773
3. Sorensen AG (2006) Magnetic resonance as a cancer imaging biomarker. J Clin Oncol 24(20):3274–3281. doi:10.1200/JCO.2006.06.6597
4. Magee T, Shapiro M, Williams D (2003) Comparison of high-field-strength versus low-field-strength MRI of the shoulder. AJR Am J Roentgenol 181(5):1211–1215. doi:10.2214/ajr.181.5.1811211
5. Schmitz BL, Aschoff AJ, Hoffmann MH, Gron G (2005) Advantages and pitfalls in 3T MR brain imaging: a pictorial review. AJNR Am J Neuroradiol 26(9):2229–2237

6. Parker GJ, Roberts C, Macdonald A, et al. (2006) Experimentally-derived functional form for a population-averaged high-temporal-resolution arterial input function for dynamic contrast-enhanced MRI. Mag Reson Med 56(5):993–1000. doi:10.1002/mrm.21066
7. Bali MA, Metens T, Denolin V, et al. (2011) Tumoral and nontumoral pancreas: correlation between quantitative dynamic contrast-enhanced MR imaging and histopathologic parameters. Radiology 261(2):456–466. doi:10.1148/radiol.11103515
8. Kim JH, Lee JM, Park JH, et al. (2013) Solid pancreatic lesions: characterization by using timing bolus dynamic contrast-enhanced MR imaging assessment: a preliminary study. Radiology 266(1):185–196. doi:10.1148/radiol.12120111
9. Klein S, Staring M, Murphy K, Viergever MA, Pluim JP (2010) elastix: a toolbox for intensity-based medical image registration. IEEE Trans Med Imaging 29(1):196–205. doi:10.1109/TMI.2009.2035616
10. Yao X, Zeng M, Wang H, et al. (2012) Evaluation of pancreatic cancer by multiple breath-hold dynamic contrast-enhanced magnetic resonance imaging at 3.0 T. Eur J Radiol 81(8):e917–e922. doi:10.1016/j.ejrad.2012.05.011
11. Zulfiqar M, Yousem DM, Lai H (2013) ADC values and prognosis of malignant astrocytomas: does lower ADC predict a worse prognosis independent of grade of tumor?: a meta-analysis. AJR Am J Roentgenol 200(3):624–629. doi:10.2214/AJR.12.8679
12. Sun XJ, Quan XY, Huang FH, Xu YK (2005) Quantitative evaluation of diffusion-weighted magnetic resonance imaging of focal hepatic lesions. World J Gastroenterol: WJG 11(41):6535–6537
13. Taouli B, Vilgrain V, Dumont E, et al. (2003) Evaluation of liver diffusion isotropy and characterization of focal hepatic lesions with two single-shot echo-planar MR imaging sequences: prospective study in 66 patients. Radiology 226(1):71–78
14. Jang KM, Kim SH, Lee SJ, et al. (2013) Differentiation of an intrapancreatic accessory spleen from a small (<3 cm) solid pancreatic tumor: value of diffusion-weighted MR imaging. Radiology 266(1):159–167. doi:10.1148/radiol.12112765
15. Rosenkrantz AB, Matza BW, Sabach A, Hajdu CH, Hindman N (2013) Pancreatic cancer: lack of association between apparent diffusion coefficient values and adverse pathological features. Clin Radiol 68(4):e191–e197. doi:10.1016/j.crad.2012.11.006
16. Dougherty G (2009) *Digital image processing for medical applications*. New York: Cambridge University Press
17. Tofts PS, Brix G, Buckley DL, et al. (1999) Estimating kinetic parameters from dynamic contrast-enhanced T(1)-weighted MRI of a diffusible tracer: standardized quantities and symbols. J Magn Reson Imaging 10(3):223–232. doi:101002/(SICI)1522-2586(199909)10:3<223::AID-JMRI2>3.0.CO;2-S
18. Blockley NP, Jiang L, Gardener AG, et al. (2008) Field strength dependence of R1 and R2* relaxivities of human whole blood to ProHance, Vasovist, and deoxyhemoglobin. Magn Reson Med 60(6):1313–1320. doi:10.1002/mrm.21792
19. Neter J, Kutner MH, Nachtsheim JC, Wasserman W (1996) *Applied linear statistical models*, 4th edn. Columbus: The McGraw-Hill Companies Inc.
20. Zwick S, Brix G, Tofts PS, et al. (2010) Simulation-based comparison of two approaches frequently used for dynamic contrast-enhanced MRI. Eur Radiol 20(2):432–442. doi:10.1007/s00330-009-1556-6
21. Heye T, Davenport MS, Horvath JJ, et al. (2013) Reproducibility of dynamic contrast-enhanced MR imaging. Part I. Perfusion characteristics in the female pelvis by using multiple computer-aided diagnosis perfusion analysis solutions. Radiology 266(3):801–811. doi:10.1148/radiol.12120278
22. Kudo K, Christensen S, Sasaki M, et al. (2013) Accuracy and reliability assessment of CT and MR perfusion analysis software using a digital phantom. Radiology 267(1):201–211. doi:10.1148/radiol.12112618
23. Tweedle MF (1997) The ProHance story: the making of a novel MRI contrast agent. Eur Radiol 7(Suppl 5):225–230
24. Fukushima N, Koopmann J, Sato N, et al. (2005) Gene expression alterations in the non-neoplastic parenchyma adjacent to infiltrating pancreatic ductal adenocarcinoma. Mod Pathol 18(6):779–787. doi:10.1038/modpathol.3800337
25. Matsuki M, Inada Y, Nakai G, et al. (2007) Diffusion-weighed MR imaging of pancreatic carcinoma. Abdom Imaging 32(4):481–483. doi:10.1007/s00261-007-9192-6
26. Balci NC, Momtahen AJ, Akduman EI, et al. (2008) Diffusion-weighted MRI of the pancreas: correlation with secretin endoscopic pancreatic function test (ePFT). Acad Radiol 15(10):1264–1268. doi:10.1016/j.acra.2008.05.002
27. Bruegel M, Holzapfel K, Gaa J, et al. (2008) Characterization of focal liver lesions by ADC measurements using a respiratory triggered diffusion-weighted single-shot echo-planar MR imaging technique. Eur Radiol 18(3):477–485. doi:10.1007/s00330-007-0785-9
28. Braithwaite AC, Dale BM, Boll DT, Merkle EM (2009) Short- and midterm reproducibility of apparent diffusion coefficient measurements at 3.0-T diffusion-weighted imaging of the abdomen. Radiology 250(2):459–465. doi:10.1148/radiol.2502080849
29. Yamada I, Aung W, Himeno Y, Nakagawa T, Shibuya H (1999) Diffusion coefficients in abdominal organs and hepatic lesions: evaluation with intravoxel incoherent motion echo-planar MR imaging. Radiology 210(3):617–623. doi:10.1148/radiology.210.3.r99fe17617
30. Hwang EJ, Cha Y, Lee AL, et al. (2013) Early response evaluation for recurrent high grade gliomas treated with bevacizumab: a volumetric analysis using diffusion-weighted imaging. J Neurooncol 112(3):427–435. doi:10.1007/s11060-013-1072-z
31. Kim HS, Kim CK, Park BK, Huh SJ, Kim B (2013) Evaluation of therapeutic response to concurrent chemoradiotherapy in patients with cervical cancer using diffusion-weighted MR imaging. J Magn Reson Imaging: JMRI 37(1):187–193. doi:10.1002/jmri.23804
32. Chopra S, Verma A, Kundu S, et al. (2012) Evaluation of diffusion-weighted imaging as a predictive marker for tumor response in patients undergoing chemoradiation for postoperative recurrences of cervical cancer. J Cancer Res Ther 8(1):68–73. doi:10.4103/0973-1482.95177
33. Chang YC, Yu CJ, Chen CM, et al. (2012) Dynamic contrast-enhanced MRI in advanced nonsmall-cell lung cancer patients treated with first-line bevacizumab, gemcitabine, and cisplatin. J Magn Reson Imaging: JMRI 36(2):387–396. doi:10.1002/jmri.23660
34. Chikui T, Kitamoto E, Kawano S, et al. (2012) Pharmacokinetic analysis based on dynamic contrast-enhanced MRI for evaluating tumor response to preoperative therapy for oral cancer. J Magn Reson Imaging: JMRI 36(3):589–597. doi:10.1002/jmri.23704
35. Kim JH, Kim CK, Park BK, et al. (2012) Dynamic contrast-enhanced 3-T MR imaging in cervical cancer before and after concurrent chemoradiotherapy. Eur Radiol 22(11):2533–2539. doi:10.1007/s00330-012-2504-4